Computers and Electrical Engineering 39 (2013) 1527–1536

Contents lists available at SciVerse ScienceDirect

Computers and Electrical Engineering

journal homepage: www.elsevier.com/locate/compeleceng

An integrated method for hemorrhage segmentation from brain CT Imaging ☆

H.S. Bhadauria [a,*], Annapurna Singh [b], M.L. Dewal [a]

[a] Department of Electrical Engineering, Indian Institute of Technology, Roorkee 247667, India
[b] Department of Computer Sc. & Engineering, G.B. Pant Engineering College, Pauri 246194, India

ARTICLE INFO

Article history:
Available online 25 May 2013

ABSTRACT

This paper presents an integrated segmentation method which combines the features of Fuzzy C-Mean (FCM) clustering and region-based active contour method. In the proposed method, FCM clustering is used to initialize the contour around the hemorrhagic region and then region-based active contour method propagates the initial contour towards the hemorrhage boundaries. Further, the FCM clustering is also used to estimate the contour propagation controlling parameters adaptively from the given image. The region-based active contour method uses the intensity information in the local regions as against the global regions in the traditional region-based active contour methods to guide the contour motion. The effectiveness of the proposed method is tested on the dataset of total 100 hemorrhagic brain CT images of 20 patients and the results are compared with region growing, FCM clustering and Chan & Vese methods. The proposed method yields the higher average values of the similarity indices namely sensitivity, specificity, accuracy and overlap metric as 79.93%, 99.10%, 84.83% and 88.84% respectively.

1. Introduction

Brain hemorrhage occurs as a result of bleeding due to leakage or rupturing of blood vessels within the brain substance. Due to high mortality and morbidity rate, brain hemorrhage detection is the primary task for the patients of the neurological disturbances and head injury. Speed of diagnosis is therefore vital, and so Computed Tomography (CT) imaging, which is faster and much less costly than other medical scans, is still the golden standard for the initial assessment. The visualization of the hemorrhagic clot on brain CT images depends on its intrinsic properties like density, volume, location, relationship to the surrounding structures and technical factors like scanning angles, slice thickness etc. [1]. Segmentation of hemorrhagic clots has crucial clinical significance because this may be useful in its prognosis and treatment trials. However, intensity inhomogeneity, irregular boundaries and worst tissue contrast may cause considerable difficulties in the hemorrhage segmentation from the brain CT images. Lots of researches have been done on medical image segmentation and two methods widely used are based on fuzzy clustering [2] and active contour [3]. In case of brain hemorrhage segmentation from brain CT images, Loncaric et al. [4,5] have largely contributed by using FCM followed by rule-based classification of the regions. Chan [6] extracts the hemorrhagic regions by using top-hat transform and left–right asymmetry. This system was capable to identify small hemorrhagic clots. Bardera et al. [7] have proposed a semi-automated segmentation method for brain hematoma and edema. Their method combines the region growing approach to segment the hematoma and level set segmentation to segment the edema. Liao et al. [8] have proposed automatic intracranial hematoma detection technique based on

☆ Reviews processed and approved for publication by Editor-in-Chief Dr. Manu Malek.

* Corresponding author.
E-mail addresses: hsb76dee@iitr.ernet.in (H.S. Bhadauria), annapurna_singh@hotmail.com (A. Singh), mohanfee@iitr.ernet.in (M.L. Dewal).

0045-7906/$ - see front matter © 2013 Elsevier Ltd. All rights reserved.
http://dx.doi.org/10.1016/j.compeleceng.2013.04.010

multi-resolution binary level set method. Their method segments the epidural and subdural hemorrhages with results comparable to human experts. Zaki et al. [9] have proposed an integrated system to extract the hemorrhage from brain CT images. Their method used the multi-level FCM to extract an intracranial structure from its background and skull and then intracranial structure is further segmented into cerebrospinal fluid, brain matter and other homogenous matters using two-level Otsu multi-thresholding method. Further hemorrhage detection is carried out by using symmetrical and pixel intensity features.

Active contour models are dynamic curves or surfaces that move within an image domain to capture desired object's boundaries. The curve motion is driven by a combination of internal and external forces, which achieve a minimal energy state when contour reaches the targeted object's boundaries. There are two main mathematical approaches for the implementation of active contours: Snakes and Geometric active contour. Snake methods [10] explicitly move predefined snake points based on energy minimization scheme while the geometric active contour methods [11] move contours implicitly as a particular level of a function. For image segmentation, geometric active contour models can be classified into two classes, viz. (i) Edge-based models and (ii) Region-based models. Edge-based models [12] use an edge detector, usually based on image gradient to attract the contour towards the desired object. Region-based active contour models identify the region of interest by using region descriptors to control the motion of the contour. Chan and Vese [13] proposed region-based model for general images by minimizing Mumford-Shah functional [14]. By incorporating the region based information into the energy function, this method has much convergence range and flexible initialization. In the traditional active contour models, it is necessary to keep the evolving level set function close to signed distance function to keep the contour smooth [15]. Thus periodic re-initialization of level set function to signed distance function during evolution has been extensively used [16]. However, as shown by Gomes and Faugeras [17], re-initialization process is quite complicated, expensive and has undesirable side effects. To overcome this problem, Li et al. [18] have proposed a model which forces the level set function closed to a signed distance function and thus eliminates the need of costly re-initialization process. Another problem with most of the active contour based segmentation methods is that their accuracy and speed largely depend upon the appropriate placement of initial contour and optimal configuration of contour propagation controlling parameters which require extensive manual intervention. Huang et al. [19] have proposed two methods in which FCM and graph-based segmentation methods are used to initialize the contour for the snake method. The method proposed in this paper an integrated segmentation technique, which not only eliminates the need of re-initialization but also initializes the active contour automatically using FCM clustering. In addition, the proposed method also estimates the contour propagation controlling parameters adaptively from the given image using the results of the FCM clustering. Further in this method, the fuzzy membership function is incorporated into the fitting functions of level set function to achieve the higher accuracy.

Section 2 presents the methodology of the proposed integrated region-based active contour method with FCM clustering, to segment the hemorrhage from brain CT images. A brief description of the standard FCM and region-based active contour method is reproduced, as the same are being used in the proposed method. The material and performance assessment parameters are discussed in Section 3. Section 4 presents the results and related observations with discussions followed by the conclusions in Section 5.

2. Methodology

The approach presented in the paper utilizes the features of both FCM clustering and region based active contour model for the segmentation of hemorrhagic regions from the brain CT images. A brief introduction of standard FCM clustering and region-based active contour model is also given in Sections 2.1 and 2.2 respectively. Section 2.3 presents the proposed approach.

2.1. Standard FCM clustering

In the last decades, fuzzy segmentation methods especially FCM [20,21] clustering have been widely used in the medical image segmentation. An image can be represented in various feature spaces, and FCM which is an unsupervised method, segments the image into objects by grouping the similar pixels in the feature space. The clustering is achieved by iterative minimization of a cost function that depends on the distance of the pixels to the cluster centers in the feature domain. Objective of image segmentation is to divide an image into meaningful regions. More formally segmentation is a process of partitioning the entire image into c crisp maximally connected regions $\{R_i\}$ such that each R_i is homogeneous with respect to some criteria. In many situations it is not easy to determine whether a pixel belongs to a region or not. To alleviate this situation, fuzzy set concepts can be used into segmentation process.

The standard FCM objective function for partitioning $\{x_k\}_{k=1}^{N}$ into c numbers of clusters is given by

$$J = \sum_{i=1}^{c}\sum_{k=1}^{N} u_{ik}^{m}\|x_k - v_i\|^2 \tag{1}$$

where x_k is the gray value of the kth pixel, v_i is the cluster center of the ith cluster, u_{ik} is the fuzzy membership of the kth pixel with respect to ith cluster and m is the parameter controlling the fuzziness of the resultant segmentation and $m = 2$ is used in this work. The fuzzy membership functions are subjected to following constraints.

$$\sum_{i=1}^{c} u_{ik} = 1 \forall k; \quad u_{ik} \in [0,1] \tag{2}$$

The membership function u_{ik} and cluster centers v_i can be calculated iteratively as

$$u_{ik} = \frac{\|x_k - v_i\|^{-2/m-1}}{\sum_{j=1}^{c} \|x_k - v_j\|^{-2/m-1}} \tag{3}$$

$$v_i = \frac{\sum_{k=1}^{N} u_{ik}^m x_k}{\sum_{k=1}^{N} u_{ik}^m} \tag{4}$$

Starting with an initial guess for each cluster center, the FCM converges to a solution for v_i representing the local minimum. The convergence can be determined by comparing the changes in the membership function or the cluster center at two successive iteration steps. After the convergence, defuzzification is applied to assign each pixel to a specific cluster for which the membership is maximal.

2.2. Region-based active contour model

The basic idea of region-based active contour models is using a level set function φ to segment an image into two regions: foreground and background. As proposed by Osher and Sethian [11], the level set function $\varphi(x,y)$, which is two dimensional Lipschitz function, represents the contour as $C = \{(x,y)/\varphi(x,y) = 0\}$, where $\varphi(x,y) > 0$ inside the contour C and $\varphi(x,y) < 0$ outside the contour C. The evolution of this contour is given by zero level function $\varphi(t,x,y)$ at time t.

In implementing the active contour models, it is necessary to reinitialize the level set function φ as a signed distance function periodically. From the practical point of view, the re-initialization process can be quite complicated, expensive and having side-effects. In order to solve re-initialization problem, Li et al. [22] have proposed a region-based model which uses intensity information in local regions at a controllable scale. The level set formulation is

$$\frac{\partial \varphi}{\partial t} = \mu\left(\nabla^2\varphi - div\left(\frac{\nabla\varphi}{|\nabla\varphi|}\right)\right) + v\delta_\varepsilon(\varphi) div\left(\frac{\nabla\varphi}{|\nabla\varphi|}\right) + \delta_\varepsilon(\varphi)(-\lambda_1 e_1 + \lambda_2 e_2) \tag{5}$$

In Eq. (5), the first term is called a penalty term, it maintains the regularity of the level set function close to signed distance function. The second term is referred to as length term and is responsible for smoothing of contour. The third term is referred to as the data fitting term and is responsible for propagating the active contour towards object boundaries. μ is the weighting coefficient of penalty term, ν is the weighting coefficient of length term and λ_1 and λ_2 are weighting coefficients of data fitting term. $\delta_\varepsilon(x)$ is smoothed Dirac function which is derivative of smooth Heaviside function $H_\varepsilon(x)$. Both these functions are defined as

$$H_\varepsilon(x) = \frac{1}{2}\left[1 + \frac{2}{\pi}\tan^{-1}\left(\frac{x}{\varepsilon}\right)\right] \tag{6}$$

$$\delta_\varepsilon(z) = \frac{1}{\pi}\frac{\varepsilon}{\varepsilon^2 + x^2} \tag{7}$$

ε is a constant which regularizes the Dirac function.

e_1 and e_2 are energy functions inside and outside C in the local regions centered at (x,y) and are defined as

$$e_1(x,y) = \int K_\sigma(s,t)|I(x+s,y+t) - f_1(x,y)|^2 dsdt \tag{8}$$

and

$$e_2(x,y) = \int K_\sigma(s,t)|I(x+s,y+t) - f_2(x,y)|^2 dsdt \tag{9}$$

f_1 and f_2 are two data fitting functions inside and outside C and are weighted averages of the intensities in the neighborhood region of (x,y)

$$f_1(x,y) = \frac{K_\sigma * [H_\varepsilon(\varphi(x,y))I(x,y)]}{K_\sigma * H_\varepsilon(\varphi(x,y))} \tag{10}$$

and

$$f_2(x,y) = \frac{K_\sigma * [(1 - H_\varepsilon(\varphi(x,y)))I(x,y)]}{K_\sigma * (1 - H_\varepsilon(\varphi(x,y)))} \tag{11}$$

K_σ is the Gaussian kernel function and is defined as

$$K_\sigma(z) = \frac{1}{(2\pi)^{n/2}\sigma^n} e^{-|z|^2/2\sigma^2} \tag{12}$$

where $\sigma > 0$ is the scale parameter which controls the size of local region. To compute the convolution in Eqs. (10), (11) more efficiently, the kernel K_σ can be truncated as a $w \times w$ mask, where w is the smallest odd number no less than 4σ. For example, for a given scale parameter $\sigma = 3.0$, $w = 13$ and the size of the mask is 13×13.

In this formulation, the level set function $\varphi_0(x,y)$ is initialized as

$$\varphi_0(x,y) = \begin{cases} c, & (x,y) \in \Omega \\ -c, & (x,y) \notin \Omega \end{cases} \tag{13}$$

where c is constant and should be larger than 2ε. Ω is the initial contour in which $\varphi_0(x,y) > 0$. The discretization of Eq. (5) can be expressed in the following iteration form

$$\varphi_{x,y}^{t+1} = \varphi_{x,y}^{t} + \tau \frac{\partial \varphi_{x,y}^{t}}{\partial t} \tag{14}$$

where τ is the time step parameter and can be taken sufficiently large. For maintaining the stable level set evaluation, the time step τ and penalty term μ must satisfy $\tau \cdot \mu < 1/4$.

2.3. Proposed fuzzy region-based active contour model

The suggested approach utilizes the features of both region-based active contour method and FCM clustering to segment the hemorrhagic regions from brain CT images. The proposed method first segments the hemorrhagic area using standard FCM clustering. At this stage, it is worthwhile to notice that the FCM segmentation method generates spurious blobs and outliers in the image. Thus the morphological operations viz. erosion and dilation have been used to get rid of these side effects. The erosion shrinks and removes the spurious blobs, and outliers and dilation expands and recovers the object of interest.

After having performed the stated morphological operations, the results of FCM clustering are used to initialize the level set function. Let $U(x,y)$ is the membership function for the fuzzy segmentation. The object of interest from the given image can be extracted as binary image $Z(x,y)$

$$Z(x,y) = \begin{cases} 1, & U(x,y) \geqslant b_0 \\ 0, & otherwise \end{cases} \tag{15}$$

$b_0 \in (0,1)$ is the adjustable threshold and for the experimentation, its value taken is 0.5.

Now the level set function can be initialized as

$$\varphi_0(x,y) = 2\varepsilon(2Z(x,y) - 1) \tag{16}$$

where ε is a constant which regularizes the Dirac function as given Eq. (7).

Further the modified data fitting functions f_1 and f_2 are proposed, with fuzzy membership matrix $U(x,y)$ is incorporated into these functions as

$$f_1(x,y) = \frac{K_\sigma * [U(x,y)H_\varepsilon(\varphi(x,y))I(x,y)]}{K_\sigma * H_\varepsilon(\varphi(x,y))} \tag{17}$$

and

$$f_2(x,y) = \frac{K_\sigma * [U(x,y)(1 - H_\varepsilon(\varphi(x,y)))I(x,y)]}{K_\sigma * (1 - H_\varepsilon(\varphi(x,y)))} \tag{18}$$

In traditional active contour methods, several controlling parameters which control the propagation of contour towards the desired object are manually inputted and their values vary from case to case. In the proposed method, all these controlling parameters are adaptively estimated from the given image using FCM clustering. The area and length of the contour produced by FCM clustering are computed using Heaviside function and Dirac function as

$$C_{Area}(\varphi \geqslant 0) = \int_\Omega H(\varphi(x,y))dxdy \tag{19}$$

$$C_{length}(\varphi = 0) = \int_\Omega \delta_0(\varphi(x,y))|\nabla\varphi(x,y)|dxdy \tag{20}$$

where Heaviside function is defined as

$$H(\varphi) = \begin{cases} 1, & if\ \varphi \geqslant 0 \\ 0, & if\ \varphi < 0 \end{cases} \tag{21}$$

and the Dirac function as

$$\delta_0(\varphi) = \frac{d}{d\varphi} H(\varphi) \tag{22}$$

As mentioned by Li et al. [18], time step of level set evolution τ in Eq. (14) may be chosen sufficiently large and the product of time step τ and regularization term coefficient μ must satisfy the condition $\tau \cdot \mu < 1/4$ for stable evolution. Thus the time step parameter τ is estimated as

$$\tau = \frac{C_{Area}}{C_{Length}} \tag{23}$$

The regularization term coefficient μ is estimated as

$$\mu < \frac{1}{4\tau} \tag{24}$$

The second term in Eq. (5) is responsible for smoothing the contour. In the proposed approach for achieving the smoother contour, the value of v is estimated as

$$v = 0.2\tau \tag{25}$$

The third term in Eq. (5) speeds up attraction of the level set function towards the desired object. This term consists of two weighting coefficients λ_1 and λ_2, over the region outside(C) and inside(C) respectively. The value of these weights should be same to lead the fair competition between the regions inside and outside the zero level contour during the evolution. Thus in the proposed approach, the value of λ_1 and λ_2 are estimated from the results of fuzzy clustering as

$$\lambda_1 = \lambda_2 = 0.5 - U(x, y) \tag{26}$$

where $U(x,y)$ is the membership function of the fuzzy clustering at each pixel of the image.

3. Material and performance evaluation parameters

To assess the effectiveness of the proposed segmentation method, it is tested on a dataset of 100 CT images of 20 patients, with 18–22 images per patient. Among these 20 patients, 11 patients are suffering with Intracerebral Hemorrhage (ICH), 5 patients are with Epidural Hemorrhage (EDH) and 4 patients are with Subdural Hemorrhage (SDH). There are total of 328 images and among them the number of images having hemorrhages is 138. This dataset was collected from Jawaharlal Nehru Medical College, Aligarh Muslim University, Aligarh, India and Amit MRI and CT Scan Center, Moradabad, India. The CT images are acquired from CT scanner manufactured by General Electric (GE) medical systems. All the images are scanned parallel to the orbito-meatal line (OML) with the exposure of peak tube voltage and tube current as 120 kV and 100 mA respectively. Each image is having the field of view (FOV) as 25×25 cm and size as 512×512, which results in a resolution of 0.49×0.49 mm^2 per pixel. The thickness of the slices is 10 mm throughout the brain.

The performance of the proposed segmentation technique is evaluated using four quantitative parameters namely Sensitivity, Specificity, Accuracy and Overlap metric. For this purpose, hemorrhage regions from CT images are manually delineated by an expert and delineated regions are taken as the ground truth. Sensitivity means percentage of hemorrhagic pixels properly included in segmentation results out of all pixels in the segmentation results. Specificity means percentage of hemorrhagic pixels properly excluded from the segmentation results out of all pixels outside of ground truth hemorrhage. Accuracy means the proportion of correctly segmented hemorrhage pixels out of all pixels of ground truth hemorrhage. These parameters are defined as follows:

$$\%Sensitivity = \left(\frac{TP}{TP + FN}\right) * 100 \tag{27}$$

$$\%Specificity = \left(\frac{TN}{TN + FP}\right) * 100 \tag{28}$$

$$\%Accuracy = \left(\frac{TP + TN}{TP + TN + FP + FN}\right) * 100 \tag{29}$$

$$\%Overlap = \left(\frac{2 * TP}{2 * TP + FP + FN}\right) * 100 \tag{30}$$

TP or True Positive means a pixel appears in both manually segmented hemorrhage area and hemorrhage area detected by computerized method. TN or True Negative means a pixel is absent from both manually segmented hemorrhage area and hemorrhage area detected by computerized method. FP or False Positive means a pixel is absent from manually segmented hemorrhage area but it appears in hemorrhage boarder detected by computerized method. FN or False Negative means a

pixel appears in manually segmented hemorrhage border but it is absent from hemorrhage border detected by computerized method [23].

4. Experimental results and discussion

To assess the effectiveness of the proposed segmentation method, it is compared with the results of Region Growing (RG), FCM Clustering and Chan and Vese (C–V) methods on a total of 100 real brain CT images, having hemorrhage of different sizes and shapes. Fig. 1 shows the results of various segmentation techniques, i.e. the final contours of the hemorrhages

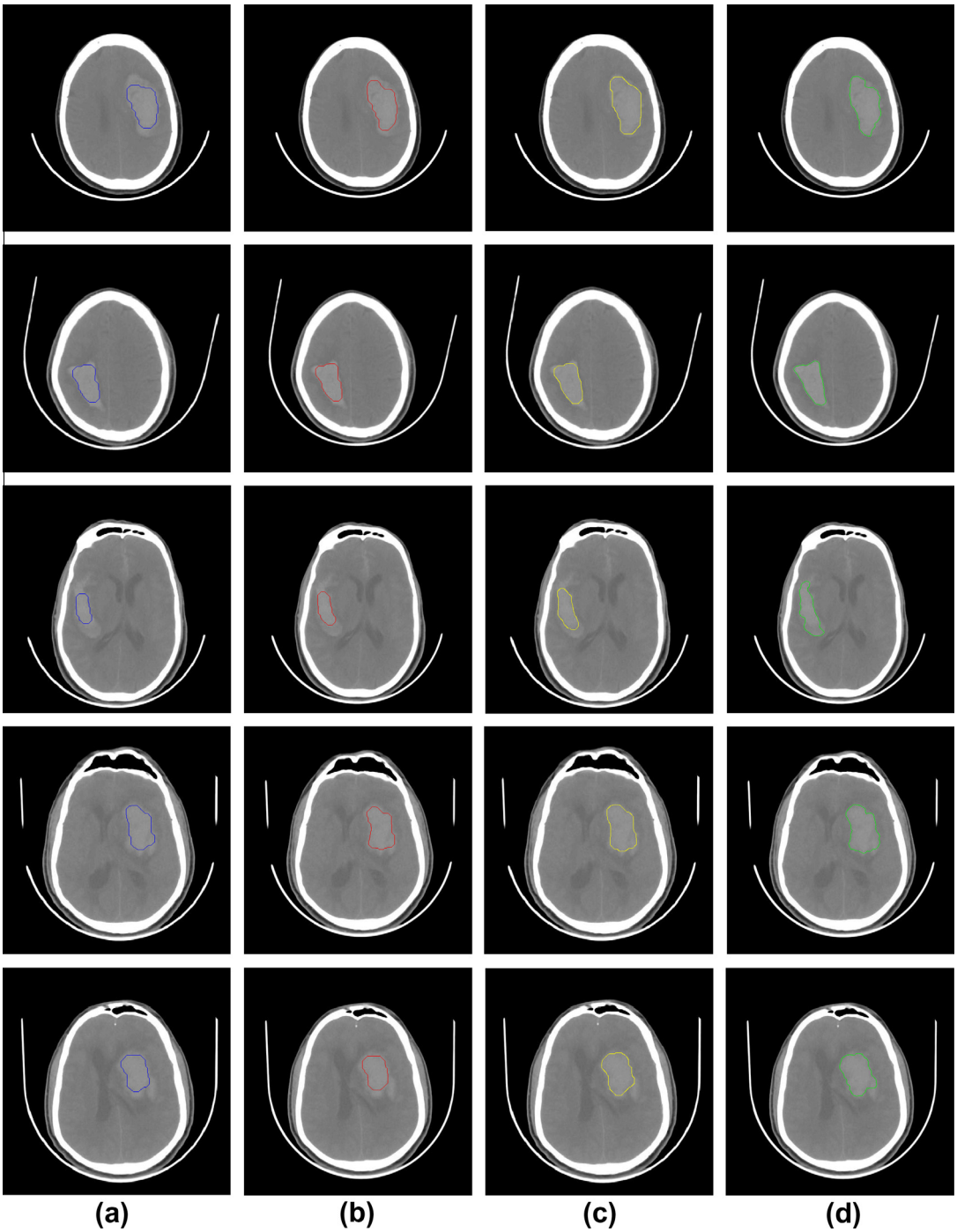

Fig. 1. Brain hemorrhage detection: column (a) region growing (b) fuzzy clustering (c) Chan and Vese (d) proposed method.

on brain CT images. It can be observed from Fig. 1 that proposed method extracts the hemorrhagic regions with the higher accuracy and outperforms all other aforementioned methodologies.

For the further analysis of the results, the hemorrhagic regions are manually delineated by the subject expert and taken as the ground truth. Table 1 shows the areas of hemorrhagic regions extracted using RG, FCM, C–V, and the proposed segmentation method when tested on a dataset of 25 CT images and their difference with respect to ground truth hemorrhagic regions. The hemorrhagic areas shown by the subject expert, i.e. ground truth regions lie in the range of 1.58–17.09 cm^2 with an average of 11.82 cm^2. The similar values for the proposed method lie in the range of 1.45–15.94 cm^2 with an average of 10.64 cm^2, for the RG method lie in the range of 1.18–14.74 cm^2 with an average of 9.03 cm^2, for the FCM method lie in the range of 1.28–15.34 cm^2 with an average of 9.91 cm^2 and for C–V method lie in the range of 1.32–14.88 cm^2 with an average of 10.14 cm^2. Thus, it is observed from Table 1 that the proposed method has produced closer segmentation results with respect to ground truth regions. Further, the average of the difference of hemorrhagic areas detected by the RG, FCM, C–V and the proposed method with respect to ground truth regions are measured on a dataset of 25 CT images, and it is observed that the proposed method yields the minimum value as 1.21 as compared to RG, FCM, and C–V, i.e. 2.79, 1.91 and 1.68 respectively. This minimum value shows higher accuracy in hemorrhage segmentation by the proposed method.

For the further analysis of the results of the proposed method, the quantitative evaluation is performed in terms of the similarity indices like sensitivity, specificity, accuracy and overlap metrics. The results of this evaluation on a dataset of 25 brain CT images are collated in Tables 2 and 3. From Table 2, it can be shown that for the proposed method, sensitivity lies in the range of 68.66–90.36 with an average value of 80.67, and specificity lies in the range of 98.27–100 with an average value of 98.58. Further, the accuracy and overlap metric are also computed and shown in Table 3. For the proposed, method accuracy lie in the range of 74.48–97.50 with an average value of 86.24 and overlap metric lie in the range of 79.59–93.66 with an average value of 87.58. For the further validation, the assessment of the proposed method along with other state-of-the-art methods is carried out on a dataset of total 100 CT images. The average values of above mentioned similarity indices for 50 and 100 images are tabulated in Tables 4 and 5. It can be observed from Tables 2–5 that the proposed segmentation method significantly improves the hemorrhage detection in terms of all similarity indices, which indicates that the proposed method extracts the hemorrhagic regions from brain CT images with higher accuracy as compared to the other methodologies.

Further the computational efficiency of the proposed method is compared with C–V method. The CPU times of these methods on 5 brain CT images are listed in Table 6. These CPU times are recorded using Matlab code run on Acer Aspire 5783 system, Intel Core 2 Duo processor, 2.2 Ghz, 4 GB RAM with Windows XP. From Table 6, it is illustrated that the proposed method yields the significant improvement in terms of computational efficiency as against the C–V method.

Radiologists usually prefer volume analysis rather than 2D segments of the hemorrhages. The computer segmentation methods provide the feasible route for the measurement of the gross hemorrhage volume from the series of 2D images.

Table 1
Comparison between different hemorrhage detection methods from brain CT images.

CT scan no.	Hemorrhagic area (cm^2)								
	Manually delineated (a)	Region growing (b)	Difference (a–b)	Fuzzy clustering (c)	Difference (a–c)	Chan and Vese method (d)	Difference (a–d)	Proposed method (e)	Difference (a–e)
1	16.72	13.68	3.04	14.55	2.17	14.8	1.92	15.58	1.14
2	11.87	7.97	3.9	9.42	2.45	9.53	2.34	10.29	1.58
3	10.78	8.62	2.16	8.99	1.79	9.08	1.7	9.55	1.23
4	16.62	12.7	3.92	13.43	3.19	13.88	2.74	15.15	1.47
5	15.44	13.95	1.49	13.83	1.61	13.87	1.57	14.39	1.05
6	17.09	14.74	2.35	15.34	1.75	14.88	2.21	15.94	1.15
7	11.08	7.74	3.34	9.25	1.83	8.95	2.13	10.21	0.87
8	11.52	7.18	4.34	9.65	1.87	9.81	1.71	10.37	1.15
9	12.46	9.16	3.3	10.64	1.82	11.59	0.87	10.86	1.6
10	15.48	13.95	1.53	13.85	1.63	14.54	0.94	14.45	1.03
11	12.52	8.22	4.3	10.63	1.89	9.33	3.19	10.93	1.59
12	10.87	6.97	3.9	8.42	2.45	8.93	1.94	8.64	2.23
13	11.4	8.16	3.24	9.6	1.8	10.72	0.68	10.86	1.54
14	12.09	8.74	3.35	9.24	2.85	9.11	2.98	10.54	1.55
15	15.62	11.65	3.97	12.35	3.27	12.64	2.98	13.73	1.89
16	14.09	10.01	4.08	13.15	0.94	13.34	0.75	13.54	0.55
17	9.78	6.58	3.2	7.99	1.79	8.13	1.65	8.57	1.21
18	10.12	8.82	1.3	8.69	1.43	9.27	0.85	9.34	0.78
19	10.14	8.82	1.32	8.62	1.52	9.07	1.07	9.45	0.69
20	13.09	11.12	1.97	12.14	0.95	13.12	0.03	12.54	0.55
21	1.72	1.22	0.5	1.28	0.44	1.32	0.4	1.47	0.25
22	11.48	9.16	2.32	9.2	2.28	9.35	2.13	9.74	1.74
23	1.58	1.18	0.4	1.32	0.26	1.39	0.19	1.45	0.13
24	9.53	6.61	2.92	7.53	2	7.8	1.73	8.19	1.34
25	12.36	8.72	3.64	8.52	3.84	8.97	3.39	10.33	2.03
Average	11.82	9.03	**2.79**	9.91	**1.91**	10.14	**1.68**	10.64	**1.21**

Table 2
Sensitivity and specificity analysis of hemorrhage detection methods on brain CT images.

Image no.	Sensitivity				Specificity			
	Region growing	Fuzzy clustering	Chan and Vese method	Proposed method	Region growing	Fuzzy clustering	Chan and Vese method	Proposed method
1	74.79	78.85	80.51	86.96	98.67	99.93	99.85	99.98
2	85.63	85.18	87.23	90.36	97.74	99.13	98.48	98.37
3	58.95	75.63	77.52	77.78	99.66	99.52	98.92	99.93
4	76.89	77.25	78.72	78.49	99.67	99.68	97.98	99.47
5	65.24	71.92	71.48	73.28	90.62	86.89	90.97	100
6	62.2	73.46	71.93	74.52	99.45	99.94	99.73	99.97
7	82.84	84.56	85.27	87.98	99.65	99.72	99.6	99.83
8	64.91	77.73	80.15	80.59	99.64	99.23	99.11	100
9	58.86	76.17	79.14	79.67	96.45	92.29	97.49	98.61
10	57.89	68.84	65.53	68.66	99.56	100	99.95	100
11	62.2	73.16	75.9	78.38	99.4	99.93	99.56	99.98
12	57.89	67.84	68.8	69.45	99.59	100	99.94	100
13	74.59	78.95	82.12	86.56	98.66	99.91	99.95	99.97
14	62.18	71.02	70.45	74.96	90.6	86.89	94.28	100
15	58.9	74.75	75.91	76.49	99.76	99.55	98.78	99.91
16	53.86	78.17	80.54	79.76	96.47	92.2	95.67	98.79
17	85.53	85.01	85.44	90.06	97.75	99.12	99.63	99.83
18	83.81	84.58	84.76	87.21	99.68	99.71	98.89	100
19	76.61	77.15	77.26	77.86	99.57	99.58	98.75	99.75
20	60.83	77.77	76.43	80.49	99.64	99.09	98.98	99.91
21	71.32	72.34	73.37	76.41	99.56	99.32	99.78	99.16
22	77.19	71.56	75.12	77.76	99.77	100	99.42	99.71
23	83.05	81.92	82.22	86.99	99.41	99.59	99.31	98.87
24	79.92	85.07	84.89	87.47	98.33	99.21	99.19	99.15
25	82.49	86.39	86.23	88.61	99.58	99.26	99.97	98.27
Average	70.34	77.41	78.28	**80.67**	98.36	97.99	98.57	**99.58**

Table 3
Accuracy and overlap measurements for hemorrhage detection methods on brain CT images.

Image no.	Accuracy				Overlap			
	Region growing	Fuzzy clustering	Chan and Vese method	Proposed method	Region growing	Fuzzy clustering	Chan and Vese method	Proposed method
1	82.56	86.87	87.83	91.42	86.42	88.1	89.43	92.14
2	84.52	84.67	86.23	87.08	91.44	91.49	91.45	93.26
3	88.85	94.32	94.29	96.11	74.29	85.34	84.93	86.06
4	76.26	76.82	77.15	77.42	86.44	86.87	86.98	87.32
5	82.88	83.19	84.06	85.83	77.68	78.14	79.67	80.59
6	74.2	72.14	73.02	84.16	77.69	84.48	85.87	85.17
7	83.59	84.24	84.44	86.73	91.25	91.75	92.31	93.1
8	75.82	77.63	79.67	82.25	76.65	87.15	88.21	89.66
9	85.24	92.99	93.23	97.5	70.63	84.05	83.79	86.24
10	78.87	77.82	78.52	79.26	73.43	80.54	80.94	81.76
11	82.19	83.11	83.56	84.13	76.69	84.47	83.32	85.14
12	87.89	87.84	88.43	89.16	73.33	80.84	81.42	81.77
13	74.56	78.88	77.42	82.28	85.43	88.19	89.54	92.13
14	72.18	72.79	73.45	74.48	76.68	77.14	78.34	79.59
15	78.85	74.41	75.43	82.31	74.09	85.33	85.89	86.56
16	82.24	83.99	84.35	85.5	68.63	85.05	87.67	86.04
17	84.15	84.27	84.87	88.08	91.4	91.46	91.43	93.66
18	83.57	84.34	82.82	86.93	91.05	91.5	92.21	93.01
19	76.06	76.82	75.63	80.28	86.4	86.89	86.8	87.34
20	80.83	87.07	88.81	90.28	75.65	87.05	88.06	89.01
21	84.42	88.73	89.72	90.54	81.6	87.41	90.53	89.6
22	85.04	84.2	84.64	86.51	82.46	81.3	81.78	84.43
23	89.79	89.9	90.1	92.24	88.64	88.78	89.39	91.6
24	91.04	92.82	91.54	93.44	90.2	92.33	92.45	93.11
25	77.37	75.49	78.86	81.97	70.93	71.81	78.7	81.3
Average	81.72	83.01	83.52	**86.24**	80.76	85.50	86.44	**87.58**

In the present work, the segmentation results of the proposed method on first slice having hemorrhage is used as the initial contour for the next slice, and this segmentation process continues till the terminal point on hemorrhage are encountered, resulting in a single pixel segment. The final contours extracted from each slice are used to estimate the gross hemorrhage

Table 4
Average sensitivity and specificity values for hemorrhage detection methods on a dataset of 25, 50 and 100 brain CT images.

Image no.	Sensitivity				Specificity			
	Region growing	Fuzzy clustering	Chan and Vese method	Proposed method	Region growing	Fuzzy clustering	Chan and Vese method	Proposed method
25	70.34	77.41	78.28	80.67	98.36	97.99	98.57	99.58
50	73.74	75.27	76.12	81.45	98.94	97.89	97.98	98.23
100	68.23	73.90	75.86	79.93	98.11	97.62	98.45	99.10

Table 5
Average accuracy and overlap values for hemorrhage detection methods on a dataset of 25, 50 and 100 brain CT images.

Image no.	Accuracy				Overlap			
	Region growing	Fuzzy clustering	Chan and Vese method	Proposed method	Region growing	Fuzzy clustering	Chan and Vese method	Proposed method
25	81.72	83.01	83.52	86.24	80.76	85.50	86.44	87.58
50	82.13	83.88	83.99	85.62	83.78	84.47	85.59	86.32
100	80.77	82.21	83.11	84.93	80.26	85.79	86.17	88.84

Table 6
Computational efficiency of proposed method (CPU times in Sec).

Method	Image 1	Image 2	Image 3	Image 4	Image 5
Chan and Vese	142.5	112.25	130.95	175.5	150.67
Proposed method	82.21	65.76	50.5	80.24	86.10

Table 7
Gross hemorrhage volume measurement using manual delineation, region growing, fuzzy clustering, Chan and Vese and proposed method.

Patient no.	Expert's diagnosis	Manually delineated (cm^3)	Region growing (cm^3)	Fuzzy clustering (cm^3)	Chen and Vese method (cm^3)	Proposed method (cm^3)
1	ICH	68.63	48.11	49.84	52.92	55.14
2	ICH	39.48	22.71	27.16	30.21	34.65
3	ICH	90.54	68.68	79.08	60.92	81.43
4	ICH	24.72	14.71	19.13	26.28	19.08
5	ICH	52.36	39.65	41.64	54.44	43.15
6	ICH	13.70	9.04	11.26	9.05	10.25
7	ICH	76.24	59.86	66.82	62.38	65.87
8	ICH	84.82	58.72	72.23	70.16	74.26
9	ICH	135.85	94.63	111.40	140.15	125.22
10	ICH	95.83	80.45	85.12	84.26	91.85
11	ICH	27.05	21.98	23.66	28.65	25.54
12	EDH	38.58	31.56	32.58	33.86	32.44
13	EDH	140.32	130.78	134.32	132.34	145.65
14	EDH	64.55	61.96	64.56	60.82	72.45
15	EDH	43.45	35.67	39.94	44.15	42.77
16	EDH	94.54	80.63	86.19	87.46	90.28
17	SDH	87.34	60.15	72.45	64.69	70.13
18	SDH	64.98	51.45	66.56	56.71	68.87
19	SDH	20.11	9.15	15.67	13.98	17.72
20	SDH	122.24	95.73	99.45	105.45	123.69

volume from the series of 2D CT images. Similarly volume measurement is also performed with the other segmentation methods like RG, FC and C–V. The results of the gross hemorrhage volume measured from various methods discussed earlier are shown in Table 7.

5. Conclusion

The identification of brain hemorrhage is one of the vital tasks because of high morbidity and mortality rate. Hemorrhage segmentation from brain CT images is the challenging task due to its weak and irregular boundaries. The measurement of hemorrhage volume from brain CT images is useful for its prognosis and treatment trials. This paper proposed an integrated

hemorrhage segmentation technique for brain CT images, which utilizes the FCM clustering to initialize the contour for the region-based active contour method and in addition, estimates the contour evolution controlling parameters automatically. The proposed method is suitable for medical images with intensity inhomogeneities because it uses the intensity information in local regions to guide the contour towards the hemorrhage boundaries. Further due to the incorporation of fuzzy membership function in fitting terms the proposed method also yields the improved robustness and accuracy for the detection of hemorrhagic regions. The results of the proposed method correlate well within the expert's measurements and may be used for clinical purposes.

References

[1] Cohen W, Wayman L. Computed tomography of intracranial hemorrhage. Neuro Imag Clinic N Am 1992;2:75–87.
[2] Pham DL, Prince JL. An adaptative fuzzy segmentation algorithm for three dimensional magnetic resonance images. Information processing in medical imaging (IPMI); 1999. p. 140–53.
[3] Caselles V, Catte F, Coll T, Dibos F. A geometric model for active contours in image processing. Numerische Mathematik 1993;66:1–31.
[4] Loncaric S, Dhawan AP, Kovacevic D, Cosic D, Broderick J, Brott T. Quantitative intracerebral brain hemorrhage analysis. Proc SPIE Med Imag 1999;3661:886–94.
[5] Loncaric S, Kovacevic D, Cosic D. Fuzzy expert system for edema segmentation. In: Proceedings of the IEEE 9th Mediterranean electro-technical conference; 1998. p. 1476–9.
[6] Chan T. Computer aided detection of small acute intracranial hemorrhage on computer tomography of brain. Int J Comput Med Imag Graphics 2007;31:285–98.
[7] Bardera A, Boada I, Feixas M, Remollo S, Blasco G, Silva Y, et al. Semi-automated method for brain hematoma and edema quantification using computed tomography. Int J Comput Med Imaging Graphics 2009;33:304–11.
[8] Liao CC, Xiao F, Wong JM, Chiang IJ. Computer aided diagnosis of intracranial hematoma with brain deformation on computed tomography. Int J Comput Med Imaging Graphics 2010;34:563–71.
[9] Zaki W, Fauzi M, Besar R, Ahamad W. Abnormalities detection in serial computed tomography brain images using multi-level segmentation approach. J Multimed Tools Appl 2011;54:321–40.
[10] Kass M, Witkin A, Terzopoulos D. Snakes: active contour models. Int'l J Comp Vision L 1987:321–31.
[11] Osher S, Sethian JA. Fronts propagating with curvature dependent speed: algorithms based on Hamilton–Jacobi formulations. J Comp Phys 1988;79:12–49.
[12] Caselles V, Kimmel R, Sapiro G. Geodesic active contour. Int'l J Comput Vision 1997;22:61–79.
[13] Chan T, Vese L. Active contours without edge. IEEE Trans Image Process 2001;10:266–77.
[14] Mumford D, Shah J. Optimal approximation by piecewise smooth function and associated variational problems. Commun Pure Appl Math 1989;42:577–685.
[15] Peng D, Merriman B, Osher S, Zhao H, Kang M. A PDE based fast local level set method. J Comp Phys 1999;155:410–38.
[16] Osher S, Fedkiw R. Level set methods and dynamic implicit surfaces. New York: Springer-Verlag; 2002.
[17] Gomes J, Faugeras O. Reconciling distance functions and level set. J Visual Commun Image Representation 2000;11:209–23.
[18] Li C, Xu C, Gui C, Fox MD. Level set evolution without re-initialization: a variational formulation. In: Proc IEEE conf computer vision and pattern recognition; 2005. p. 430–6.
[19] Huang QH, Lee SY, Liu LZ, Lu MH, Jin MH, Li AH. A robust graph-based segmentation method for breast tumors in ultrasound images. Ultrasonics 2012;52:266–75.
[20] Bezdek JC, Pal SK. Fuzzy models for pattern recognition. Piscataway, NJ: IEEE Press; 1991.
[21] Chuang KS, Tzeng HL, Chen S, Wu J, Chen TJ. Fuzzy c-means clustering with spatial information for image segmentation. Comput Med Imag Graphics 2006;30:9–15.
[22] Li C, Kao CY, Gore JC, Ding Z. Minimization of region-scalable fitting energy for image segmentation. IEEE Trans Image Process 2008;17(10):1940–9.
[23] Metz C. Basic principles of ROC analysis. Semin Nucl Med 1978;8:283–98.

H.S. Bhadauria B.Tech. (1999) (Computer Science & Engineering), M. Tech. (2004) (Electronics Engineering) both from Aligarh Muslim University, Aligarh; did his Ph.D. (2013) from Indian Institute of Technology, Roorkee, India. He has published some 20 research papers in International and National Journals and Conferences. His areas of Interest are Digital Image and Digital Signal Processing.

Annapurna Singh M.Tech. (2003) from Banasthali Vidyapeeth, Banasthali, India; did her Ph.D. (2012) from Uttarakhand Technical University, Dehradun in Computer Science Engineering. From 2003 to till date she worked as lecturer in various Engineering Colleges of India and presently working as an Assistant Professor in Computer Science Engineering of G.B. Pant Engineering College, India.

M.L. Dewal B.Tech. (1972) (Electrical Engineering) from G.B. Pant University of Agriculture and Technology, Pantnagar, US Nagar, India; did his M.E. (1974) and Ph.D. (1982) both in Electrical Engineering from Indian Institute of Technology, Roorkee. Dr. Dewal has served the University of Technology, Baghdad, Iraq, as Associate Professor and as Technical Manager of two Major Power and Desalination Plants, Ghubrah and Russail, Muscat, Sultanate of Oman during the years 1988–1991 and 1996–1997, respectively. He continues to be faculty in Electrical Engineering Department, Indian Institute of Technology, Roorkee, India since 1974.